INTERFEROMETRIC INVESTIGATIONS WITH THE SENTINEL-1 CONSTELLATION

Pau Prats-Iraola[a], Matteo Nannini[a], Nestor Yague-Martinez[a], Muriel Pinheiro[a], Jun-Su Kim[a]
Francesco Vecchioli[b], Federico Minati[b], Mario Costantini[b], Sven Borgstrom[c],Prospero De Martino[c],
Valeria Siniscalchi[c], Michael Foumelis[d], Yves-Louis Desnos[e]

[a] German Aerospace Center (DLR), Microwaves and Radar Institute, Germany
[b] e-GEOS SpA, ASI/Telespazio, Italy
[c] National Institute of Geophysics and Volcanology (INGV), Vesuvius Observatory, Italy
[d] French Geological Survey (BRGM), France
[e] ESA-ESRIN, EO Science, Applications and Future Technologies Department, Italy

ABSTRACT

The contribution focuses on the current status of the ESA study entitled "INSARAP Sentinel-1 Constellation Study", which investigates the interferometric performance of the S1A/S1B units. General aspects like the interferometric compatibility in terms of common range and Doppler bandwidth and the burst synchronization are addressed. Besides the first interferometric results with both units, time series results over the pilot sites combining both satellites are also shown, as well as some investigations with fast moving (i.e., glaciers) scenarios.

Index Terms— Sentinel-1, TOPS Interferometry, coregistration, time series

1. INTRODUCTION

The European Space Agency's (ESA) Sentinel-1A (S1A) and Sentinel-1B (S1B) satellites were successfully launched on April 3rd, 2014, and April 25nd, 2016, respectively. Both units are operated with a 180 deg shift in the same orbital plane in order to reduce the repeat-pass cycle from 12 days to 6 days. This contribution presents several results demonstrating the excellent interferometric compatibility between both units.

The main operational mode of both satellites, the Interferometric Wide swath (IW) mode operated as TOPS mode, provides a large swath width of 250 km at a ground resolution of 5x20m in range and azimuth, respectively [1]. The technical aspects related to a proper interferometric processing of TOPS data have been deeply analyzed leading to a solid processing strategy [2, 3, 4, 5].

Section 2 presents the results related to the interferometric compatibility between both units, mainly focused on the azimuth common bandwidth and the effective baseline. Section 3.1 shows the first InSAR results obtained after Sentinel-1B reached the reference orbit. Section 3.2 presents time series results over the pilot site of Campi Flegrei and Section 3.3 presents some investigations over glaciers in order to mitigate phase jumps between bursts in the presence of azimuthal motion in the scene.

This work was supported in part by the European Space Agency's SEOM Programme under Contract 4000110587/14/I-BG.

2. INTERFEROMETRIC PERFORMANCE

A temporal analysis has been carried out by systematically seeking interferometric pairs with S1B annotation files and interferometric pairs combining S1A and S1B annotation files. A total of 16444 S1A and 11048 annotation files in IW mode in the period from mid-June 2016 until beginning of September 2016 were explored. The search of interferometric pairs provided a total of 419 interferometric pairs of acquisitions employing S1A and S1B and 799 interferometric pairs of employing S1B. In the first place the mean Doppler centroid frequency employing each acquisition along the time is summarized in Fig. 1(left). It can be seen that the mean Doppler frequency of Sentinel-1A is located around 0 Hz whereas Sentinel-1B presented a mis-pointing that was corrected at the beginning of September, presenting from this date on values closer to 0 Hz, as expected. Fig. 1(right) shows the radius of the baseline between S1A and S1B from June until November 2016. The values prove the excellent orbit control of the two units to keep the orbital tube as specified by the requirements, both in terms of the across-track component and the along-track one, the latter being relevant to keep the burst synchronization of long data takes [6].

Fig. 2(left) shows the evaluated burst mis-synchronization between S1A and S1B. The standard deviation is 4.66 ms, which is within the specifications. Note that there are several outliers, probably due to manoeuvres and corrections during the commissioning phase. Fig. 2(right) shows the common Doppler bandwidth for interferometric pairs with the S1B unit. The common bandwidth is in most cases larger than 95%. The outliers are probably due to the changes in the

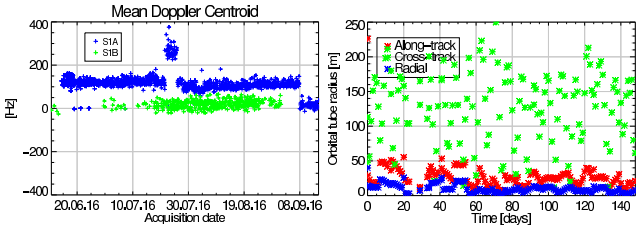

Fig. 1. (Left) Mean Doppler centroid for S1A and S1B. Beginning of September the pointing of S1B was corrected. (Right) S1A-S1B Baseline tube computed from the restituted orbits. The dimensions agree with the expected orbital tube.

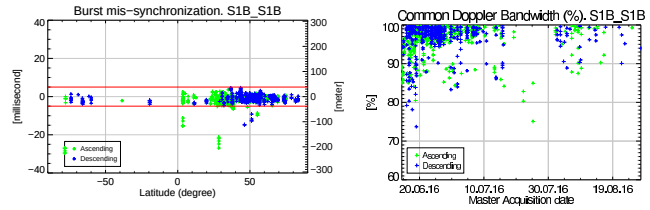

Fig. 2. (Left) Burst mis-syncrhonization between S1A and S1B. (Right) Common Doppler bandwidth for S1B interferometric pairs. The common bandwidth is in most cases greater than 95%.

attitude that can be observed in Fig. 2(left).

3. INTERFEROMETRIC RESULTS

3.1. First Cross-InSAR Results

In this section, some of the first interferograms computed during the S1B commissioning phase are shown. The main goal was to evaluate whether a proper combination of S1A and S1B images was possible without observing artifacts, especially in the phase, which is more sensitive to errors in the calibration of certain aspects like for example, the phase of the elevation antenna pattern. Fig. 3 shows the first cross-interferogram between S1A and S1B computed in the frame of the commissioning phase, which was acquired over Romania the day S1B reached its reference orbit with the correct phasing of 180° with respect to S1A. The S1A acquisition was performed on June 10th and the S1B one on June 16th. Fig. 4 shows a second cross-interferogram, in this case consisting of a long data take (8 slices) acquired over east Europe. The acquisitions were performed on June 13th and June 19th by S1A and S1B, respectively.

The visual inspection of these interferograms reveals the very good accuracy of the restituted and precise orbit data, since no residual fringes due to orbit inaccuracies can be observed. This fact already points to accuracies in the centimeter range for the orbit products. Also, no visual phase jumps could be observed between burst, hence confirming that ESD could properly estimate the residual azimuth coregistration error and correct for it. Note that the interferograms have been flattened employing an SRTM DEM, and therefore the residual fringes are mainly due to atmospheric artifacts. Additionally, the visual inspection shows no phase jumps between subswaths. This fact confirms the gut calibration of the antenna pattern phase.

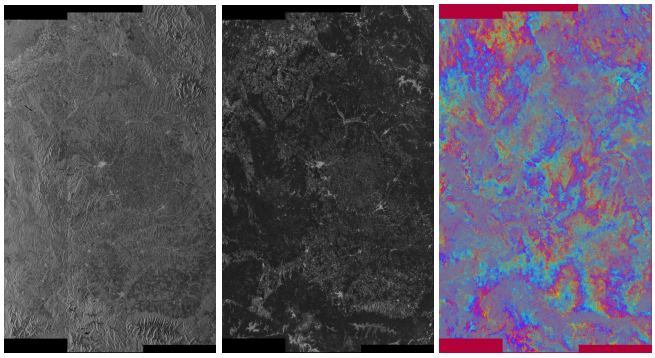

Fig. 3. Sentinel-1A/B cross-interferogram acquired over Romania: (Left) Reflectivity image, (middle) coherence and (right) phase. The Sentinel-1A/B images were acquired on June 10th (S1A) and June 16th, 2016 (S1B), shortly after S1B hat reached its reference orbit.

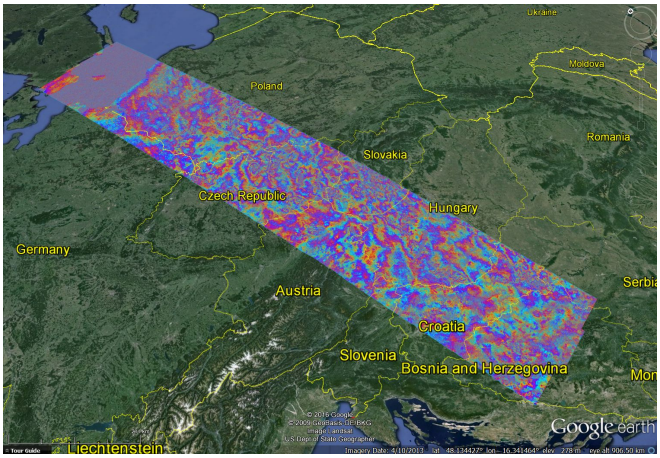

Fig. 4. S1A/S1B cross-interferogram over East Europe overlaid over Google Earth. The length of the data takes is about 1400 km.

Another example representative for deformation monitoring is shown in Fig. 5, where a S1A/S1B cross-interferogram is generated with a temporal baseline of six months (December 2015 for S1A and June 2016 for S1B). The data takes are over Mexico City, and due to the large time span, the deformation fringes due to ground water extraction and soil compaction over the city can be clearly appreciated.

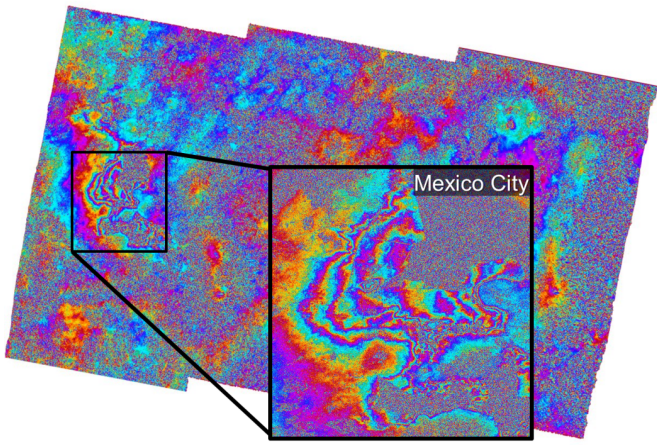

Fig. 5. S1A/S1B cross-interferogram over Mexico City with a time baseline of six months, clearly showing the fringes due to subsidence.

3.2. Time Series Results

This section is dedicated to the PSI analysis over the pilot site of Campi Flegrei. The time series acquired over this test site spans over two years, including 5 months of S1B images (from October 2016 until February 2017). The mean deformation velocity maps of the complete IW mode swath for the ascending and descending geometries are presented in Fig. 6. The uplift currently taking place at the Campi Flegrei caldera can be clearly observed and is in good agreement with the geodetic measurements [7]. In the descending configuration the landslide of Maratea can be also observed (see Fig. 8).

The east-west and vertical inversion of the deformation time series has been also performed. Fig. 7 shows a close-up of the deformation maps over the Campi Flegrei caldera. The observed measurements are in good agreement with the deformation measured with cGPS stations [7]. Due to the current inflation process at the caldera, a clear uplift is taking place, with the corresponding east and west displacements.

3.3. Refined Processing for Glaciers

In fast-moving scenarios, e.g., glaciers, the azimuthal motion of the scene introduces undesired phase jumps between bursts that could impair the phase unwrapping process along consecutive bursts. As presented in [8], one possible approach to mitigate these phase jumps is to estimate the azimuth offsets by exploiting cross-correlation and spectral diversity sequentially. This approach requires a large averaging spatial window in order to achieve the required accuracy, hence not being adaptive to local displacements, and being also very sensitive to low coherent areas. For the particular case of glaciers, one additional approach would be to make the surface-parallel-flow assumption, and further assume that the flow is in the

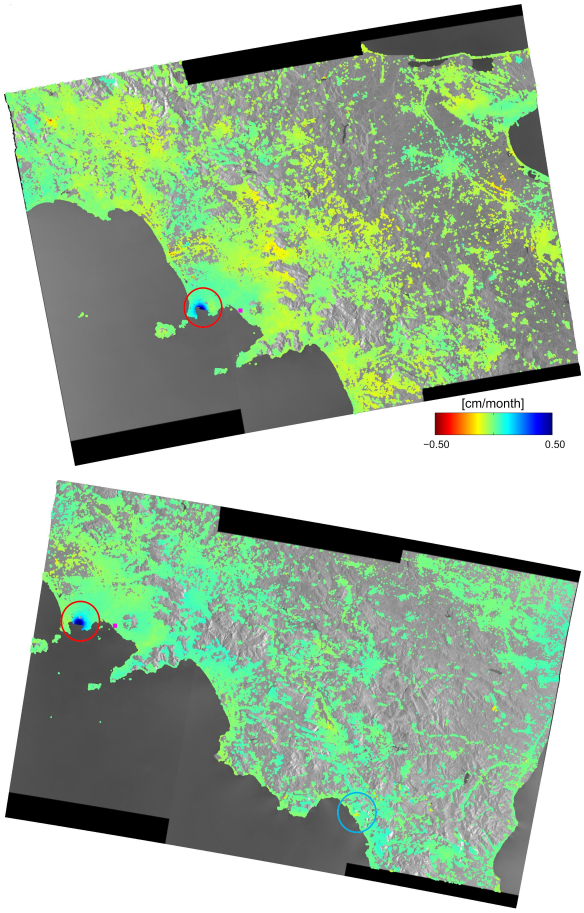

Fig. 6. Mean deformation velocity over the Campi Flegrei area for the (top) ascending and (bottom) descending configurations. The red circles indicate the location of the Campi Flegrei caldera, while the blue circle in the descending configuration indicates the location of the landslide at the city of Maratea.

direction of maximum gradient. Therefore, with the use of an external DEM, one can estimate the 3D motion from one single measurement. In the present case, the range measurements have been re-projected in the direction of maximum gradient of the topography computed with the TanDEM-X DEM. Fig. 9 shows the results of the evaluation over a glacier in the Northeast of Greenland. The original phase (left image) clearly shows phase jumps between bursts due to the azimuthal motion. After applying [8], the noisy estimation of the azimuth shifts introduces phase biases, especially at burst edges, where the Doppler centroid is larger (middle image). The proposed approach (right image) mitigates most of the phase jumps, while a couple of artifacts due to some unfiltered outliers in the estimation of the range offsets can be appreciated. In any case, the final result represents an improvement w.r.t. the original phase.

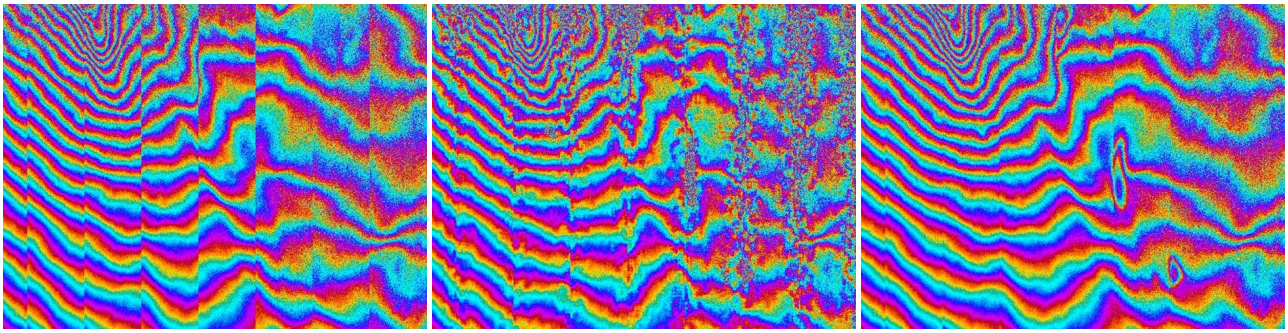

Fig. 9. Differential phase over a Greenland glacier. The phase jumps between bursts occur due to the presence of azimuthal motion in the scene. (Left) Original phase, (middle) after following the approach in [8], (right) after using the proposed approach. Azimuth is horizontal.

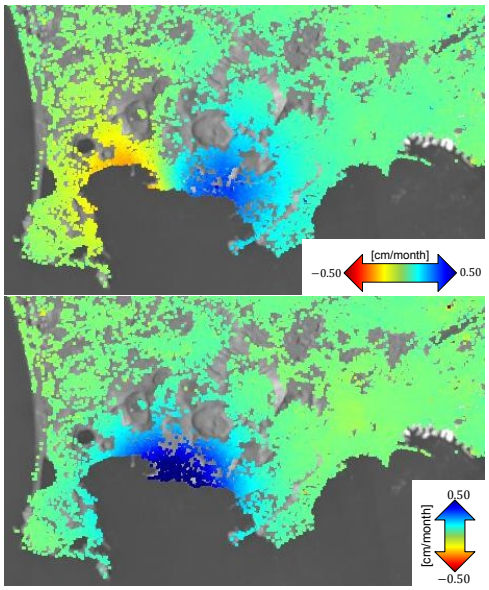

Fig. 7. Close-ups over the Campi Flegrei caldera for the (top) east-west and (bottom) vertical deformation velocity maps. The displacements show the current inflation process at the caldera, with an uplift and horizontal motion.

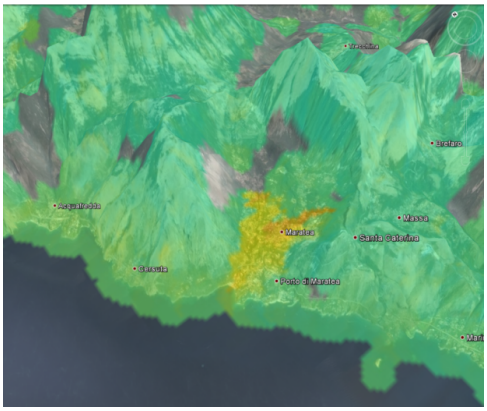

Fig. 8. Landslide on the city of Maratea overlaid with a 3D Google Earth model. Same color scale as in Fig. 6.

4. SUMMARY

This contribution has presented several results obtained with the S1A/S1B constellation, which demonstrate the excellent interferometric compatibility between the two units. The results include some of the first cross-interferograms and the evaluation of the time series over Campi Flegrei, where five months of S1B where included in the PSI processing. Some on-going investigations related to the mitigation of phase jumps between bursts over glaciers have been also presented.

5. REFERENCES

[1] R. Torres, P. Snoeij, D. Geudtner, D. Bibby, M. Davidson, E. Attema, P. Potin, et al., "GMES Sentinel-1 mission," *Remote Sensing of Environment*, vol. 120, pp. 9–24, 2012.

[2] Pau Prats-Iraola, Rolf Scheiber, Luca Marotti, Steffen Wollstadt, and Andreas Reigber, "TOPS interferometry with TerraSAR-X," *IEEE Trans. Geosci. Remote Sens.*, vol. 50, no. 8, pp. 3179–3188, 2012.

[3] "InSARap workshop, 10–11 December 2014, Frascati, Italy," http://seom.esa.int/insarap/.

[4] "Fringe workshop," 2015, http://seom.esa.int/fringe2015/.

[5] Nestor Yague-Martinez, Pau Prats-Iraola, Fernando Rodriguez Gonzalez, Ramon Brcic, Robert Shau, Dirk Geudtner, Michael Eineder, and Richard Bamler, "Interferometric processing of Sentinel-1 TOPS data," *IEEE Trans. Geosci. Remote Sens.*, vol. 54, no. 4, pp. 2220–2234, 2016.

[6] P. Prats-Iraola, M. Rodriguez-Cassola, F. De Zan, R. Scheiber, P. Lopez-Dekker, I. Barat, and D. Geudtner, "Role of the orbital tube in interferometric spaceborne SAR missions," *IEEE Geosci. Remote Sens. Lett.*, vol. 12, no. 7, pp. 1486–1490, July 2015.

[7] "INGV web page with the official bulletin from campi flegrei," http://www.ov.ingv.it/ov/it/bollettini/272-campi-flegrei-bollettini-settimanali.html.

[8] R. Scheiber, M. Jaeger, P. Prats-Iraola, F. De Zan, and D. Geudtner, "Speckle tracking and interferometric processing of TerraSAR-X TOPS data for mapping nonstationary scenarios," *IEEE JSTARS*, 2014, to be published.